Elucidating the Dynamics of Polymer Transport through Nanopores using Asymmetric Salt Concentrations

Martin Charron,‡ Lucas Philipp,‡ Liqun He, Vincent Tabard-Cossa

150 Louis-Pasteur Private, Department of Physics, University of Ottawa, Ottawa K1N 6N5, Canada

‡M.C. and L.P. contributed equally.

Address correspondence to tcossa@uottawa.ca

Abstract

While notable progress has been made in recent years both experimentally and theoretically in understanding the highly complex dynamics of polymer capture and transport through nanopores, there remains significant disagreement between experimental observation and theoretical prediction that needs to be resolved. Asymmetric salt concentrations, where the concentrations of ions on each side of the membrane are different, can be used to enhance capture rates and prolong translocation times of electrophoretically driven polymers translocating through a nanopore from the low salt concentration reservoir, which are both attractive features for single-molecule analysis. However, since asymmetric salt concentrations affect the electrophoretic pull inside and outside the pore differently, it also offers a useful control parameter to elucidate the otherwise inseparable

physics of the capture and translocation process. In this work, we attempt to paint a complete picture of the dynamics of polymer capture and translocation in both symmetric and asymmetric salt concentration conditions by reporting the dependence of multiple translocation metrics on voltage, polymer length, and salt concentration gradient. Using asymmetric salt concentration conditions, we experimentally observe the predictions of tension propagation theory, and infer the significant impact of the electric field outside the pore in capturing polymers and in altering polymer conformations prior to translocation.

Keywords: Nanopore, DNA Translocation, Salt Gradient, Tension Propagation, Polymer Transport

1. Introduction

Elucidating the physics that govern nanopore transport phenomena is a fertile field of research and is important for increasing our ability to design strategies for controlling molecular passage from which numerous technological applications can be built. On top of the spectacular innovations in DNA sequencing technology [1–5], nanopores promise radical advances in the life sciences and medicine with ultra-sensitive, point-of-care diagnosis of disease [6–12], identification and sequencing of proteins [13–19], and in next-generation information storage with decoding of digital data from sequence-controlled polymers [20–22]. To date however, while multiple theories have been developed to describe both the capture [23,24] and translocation [25–30] processes, only a few experimental studies [31–37] have attempted to validate the proposed concepts, with varying degrees of agreement. This is in large part due to the complex nature of the translocation dynamics, which occur as a multi-step, highly non-equilibrium process dictated mainly by forces over which experimental control has been challenging or impossible, making verification of theoretical ideas particularly difficult. Only just recently has the first clear experimental

confirmation of tension-propagation theory been provided, obtained through the measurement of the two-step, non-constant and non-monotonic velocity profile of nanostructured DNA molecules undergoing translocation [38]. Further experimental work is however needed to provide a more complete picture of the dynamics of polymer transport and to deliver better insights on how to design or improve many sensing and sequencing schemes.

Asymmetric salt concentration (ASC) conditions, in which a nanopore separates two reservoirs of different salt concentrations, offer a flexible method to probe the dynamics of transport through nanopores. Previous publications have shown that ASC conditions provide a simple method by which to decouple capture rate and translocation velocity; Measurements with molecules in the *cis* side being in a lower salt concentration than the *trans* side ($C_{trans}/C_{cis} > 1$) have revealed both increased capture rates and decreased translocation velocities [37,39–45], whereas these quantities are positively correlated when modulated by other standard means (*e.g.* tuning the voltage, salt concentration [46,47], pore size [36,47] or temperature [48]).

In this work, we use ASC conditions as a sensitive method to modulate the different forces impacting the capture and translocation of double-stranded DNA fragments through solid-state nanopores in the 5 to 10 nm pore size range, made in ~10 nm thick silicon nitride membranes. For different ASC conditions, we report the dependence on applied voltage, DNA length, and salt concentration ratio of multiple metrics including capture rate, mean and standard deviation of translocation times. In doing so, we reveal that the underlying physics governing the capture and translocation processes under ASC conditions are fundamentally the same as in symmetric salt concentration (SSC) conditions, though the magnitude and balance of forces inside and outside the pore differ due to salt-gradient induced changes in the electric field profile, electrophoretic

mobility throughout the system, and to the appearance of diffusioosmotic and diffusiophoretic forces.

Briefly, we find that capture in ASC conditions is described by the same two regimes found in SSC conditions, namely the diffusion- and barrier-limited regimes [24], but that ASC conditions modulate the voltage and polymer length at which capture transitions from one regime to the other. We then validate that the translocation times scale with voltage and polymer-length as postulated by iso-flux tension propagation formalisms [28], but reveal different scaling exponents between ASC and SSC conditions. Using higher-order translocation time statistics, we further demonstrate that ASC conditions alter polymer conformations and elongations prior to translocation, which helps explain the different translocation time scalings observed in ASC and SSC conditions. These results highlight the dual effect of the non-uniform forces outside the pore in first elongating polymers before their arrival at the pore entrance and then compressing them against the nanopore membrane prior to the start of their translocation [49–52]. The depth of the data presented provides experimental confirmation of previously proposed theoretical concepts, and delivers new insights to design ways to control the motion and capture of biological or synthetic polymers.

2. Results and Discussion

Before presenting the main experimental results, we first provide an overview of the different forces present for the experimental conditions used in this work, in which both an electric potential and a salt concentration gradient are used to generate polymer capture and translocation. Here, since all experiments were performed in solutions buffered at pH 8, which is above the isoelectric point of our silicon nitride membranes and of double stranded DNA (dsDNA), we

expect both electroosmotic and diffusioosmotic phenomena to be relevant to the polymer transport dynamics.

Electrophoresis & Electroosmosis - In a typical experiment under SSC conditions, the application of a voltage difference between the *cis* and the *trans* side results in most of the electric potential dropping inside the nanopore, i.e. the electric field is highest in the pore. Outside the nanopore, the potential drops as ~1/r, or equivalently the electric field decays as ~1/r^2 [24,53,54]. The high electric field inside the pore, and the negatively charged pore walls lead to an electroosmotic flow (EOF) in the direction of the field, along the nanopore length, induced by the motion of positive counterions accumulated at the pore wall. Outside the pore, the EOF velocity should decay as ~1/r^2, due to fluid flow continuity [55]. Therefore, since dsDNA is also negatively charged, its velocity anywhere in the system has an electrophoretic contribution v_{EP}, due to the electric field's pull on the charged polymer, and an EOF contribution v_{EO}, due to the convective fluid flow induced by the charged pore surface, with both contributions being in opposite directions (see Figure 1a). For charged dsDNA and SiN membrane type used here, electrophoresis dominates (i.e. $v_{EP} > v_{EO}$) and dsDNA molecules move in the direction opposite the electric field.

Diffusiophoresis and Diffusioosmosis - Recently, McMullen *et al.* [56] showed that DNA translocation could be achieved under ASC conditions without the need of an applied voltage. Under a salt gradient, the salt-concentration profile should be very similar to that of the electric potential profile under symmetric conditions described above, since to first order the quasi-steady state diffusion equation $\nabla^2 C = 0$ and Poisson equation $\nabla^2 V = 0$ are identical, assuming no convective flow and no charge. For this reason, most of the salt-concentration change is expected to occur inside the nanopore, while concentrations outside the pore to decay as ~1/r to the respective values of the *cis*- and *trans*-side salt concentrations C_{cis} and C_{trans} [57]. Because of the

sharp salt-concentration change inside the pore and of the negatively charged walls, a diffusioosmotic flow is expected to form from the high- to the low-concentration reservoir, as experimentally observed in nanochannels by Lee *et al* [58]. Such a convective fluid flow arises when an electrolyte gradient is present along the length of a charged surface, partly due to the different diffusivities of anions and cations inducing an electric field tangent to the pore walls, and due to the osmotic pressure gradient within the double layer [58,59]. Again, because of fluid flow continuity the diffusioosmotic-flow velocity outside the pore is expected decay approximately as ~$1/r^2$. Moreover, since dsDNA is negatively charged and mobile, it feels a diffusiophoretic force opposing the diffusioosmotic solvent force, akin to electrophoresis and electroosmosis. The velocity of dsDNA anywhere in this system therefore has a diffusiophoretic contribution v_{DP}, due to dsDNA probing the non-uniform salt concentration profile, and a diffusioosmotic flow contribution v_{DO}, due to the convective flow induced by the charged pore surface, with both contributions being in opposite directions, as depicted in Figure 1b.

Since both electric biases and salt gradients are used to induce DNA capture and translocation in this work, the velocity of DNA at any point in the system is expected to have contributions from electrophoresis, electroosmosis, diffusiophoresis and diffusioosmosis, as discussed above: $\vec{v} = \vec{v}_{EP} + \vec{v}_{EO} + \vec{v}_{DP} + \vec{v}_{DO}$. It should further be noted that salt gradients modulate non-uniformly the electrophoretic mobility and the electric field inside and outside the nanopore system. The former is a direct result of electrophoretic mobility's dependence on ionic concentration, whereas the latter is best understood by modeling the nanopore system as three resistors in series, i.e. one resistor for the cylindrical nanopore R_{pore}, and two for the *cis*- and *trans*-side access regions, and R_{cis} and R_{trans} (Figure 1c). For example, increasing the salt concentration in the *trans*-reservoir also increases the concentration inside the pore, and therefore reduces the

trans-side and pore resistances and voltage drops. To conserve the total applied voltage of the system, the voltage and electric field on the *cis* side increase. Lastly, salt gradients are known to induce an electrochemical potential difference between the electrodes in addition to the intended applied bias [56]. To better compare ASC and SSC conditions, this electrochemical bias was compensated before each experiment by applying an offset voltage in order to zero the ionic current. The voltages reported below are therefore measured with respect to this initial potential offset.

Nanopore Capture and Translocation Steps

The capture and translocation of polymers into nanopores is a complex nonequilibrium process resulting from coupled electrohydrodynamic and diffusion processes which occur on a wide variety of timescales spanning both sides of the polymer relaxation time. In SSC conditions, i.e. with no salt gradient, the electric field inside and outside the pore drives most of the directed transport mechanisms [23,24]. In ASC conditions however, additional diffusioosmotic forces are expected to impact the dynamics of capture and translocation. Because of the qualitative similarities between electrophoretic and diffusioosmotic forces outlined above (i.e. forces strongest inside pore, and decaying outside pore), the complete capture and translocation process of a polymer in both SSC and ASC conditions can be described using the five following steps: i) The polymer diffuses from the solution bulk close to the nanopore capture volume, a hemisphere-like volume inside which the force-induced drift (Figure 1d) is stronger than thermal motion [37,53,54]; ii) The polymer drifts towards the pore, during which it is elongated by the force gradient [49–51], until it arrives at the pore; iii) The polymer at the pore entrance is compressed against the nanopore membrane by the forces until threading begins either by an end or a folded segment of the polymer [50,51]; iv) Due to the high pulling force inside the pore, the polymer

undergoes non-equilibrium deformation during translocation. As consecutive segments are pulled inside the pore, the fraction of the polymer still on the *cis*-side is being deformed with a growing mobile segment as the tension propagates along its contour length [26–28,38,60,61]; v) Once the tension reaches the polymer end, the polymer continues translocation but with a shrinking *cis*-side segment fully under tension until the polymer is fully threaded [26–28,38,60,61].

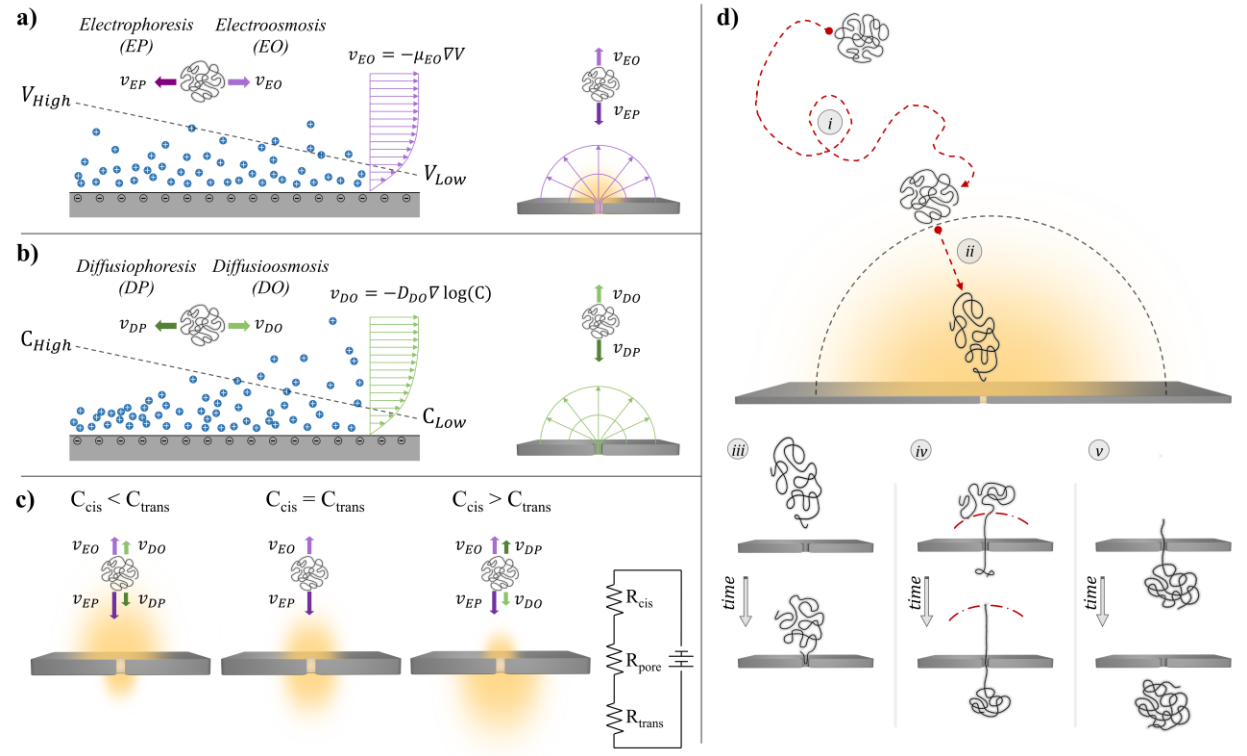

Figure 1. (a) Schematic of the effect of an applied electric potential difference on a charged polymer near a charged membrane (left), and on a charged polymer outside a nanopore (right). **(b)** Schematic of the effect of an electrolyte concentration gradient on a charged polymer near a negatively charged membrane (left), and a charged polymer outside a nanopore (right). **(c)** Schematic of the direction of forces present under an applied electric bias and three different salt concentration gradients. The yellow hemispheres are used to depict the modulation of electric field strengths. **(d)** Schematic of the capture and translocation steps: (i) Polymer diffuses close to the pore; (ii) Polymer drifts to the pore mouth; (iii) Polymer segment finds and enters the pore, thereby initiating translocation; (iv) Tension propagation: A growing fraction of the polymer is under tension/motion. The tension front is represented by a red dashed line; (v) Post-propagation: All monomers on *cis*-side move towards the pore;

Note that only the strongly driven translocation regime has been described above, and not the weakly driven regime [62], in which the translocation steps *iv* and *v* occur on timescales comparable to or longer than the relaxation time of the polymer. Since the majority of experimental work with solid-state nanopores occurs in the strongly driven regime [38], we focus our efforts there.

Capture Scaling

In order to investigate how the capture process is affected by different ASC conditions, we first describe the scaling of capture rate with applied voltage (ΔV) and polymer length (N) in both ASC and SSC conditions. As described elsewhere, capture rate in standard SSC conditions is well described by both the barrier-limited regime for short polymers or low voltages, and by the diffusion-limited regime for long polymers or high voltages (also termed drift-limited regime [23,32]), in which the rate-limiting step is the polymer overcoming a largely entropic, free-energy barrier or diffusing into the capture volume, respectively [23,24,53,63].

$$R \equiv \frac{J}{c} \propto \begin{cases} N^{\gamma} e^{\delta \Delta V}, & N, \Delta V < N^*, \Delta V^* \\ \mu_e \Delta V, & N, \Delta V > N^*, \Delta V^* \end{cases} \quad (1)$$

Here, R is the normalized capture rate, defined as the ratio of capture rate J and polymer concentration c, μ_e is the electrophoretic mobility of the charged polymer, and γ and δ are scaling coefficients. The regime-transition polymer length and voltage values are denoted by $N^*$and ΔV^*, are interdependent, and both depend strongly on experimental parameters [23,24]. Note that since we use double-stranded DNA (dsDNA) as our model linear polymer, and its electrophoretic

mobility is length independent above a few hundred bases [64], its capture rate is expected to scale as $R \sim N^0 \Delta V^1$ in the diffusion-limited regime [32,33,37].

To test the validity of the voltage scaling of Equation 1 for polymer capture in ASC conditions, we performed experiments using 0.25 nM of 10,000 base pairs (bp) dsDNA in a 5.3 nm diameter nanopore, under applied voltages ranging from 50 mV to 600 mV, in three different LiCl salt conditions: SSC (C_{trans}/C_{cis}= 0.45 M/0.45 M = 1); capture-promoting ASC (C_{trans}/C_{cis} = 3.6 M/0.45 M > 1); and capture-opposing ASC (C_{trans}/C_{cis} = 0.45 M/3.2 M < 1). Figures 2a-c show representative current traces acquired under a bias of 400 mV in SSC, capture-promoting and capture-opposing ASC conditions, respectively. At each voltage, the inter-event time distribution was extracted, and the corresponding capture rate was determined [33], as shown in Figure 2d.

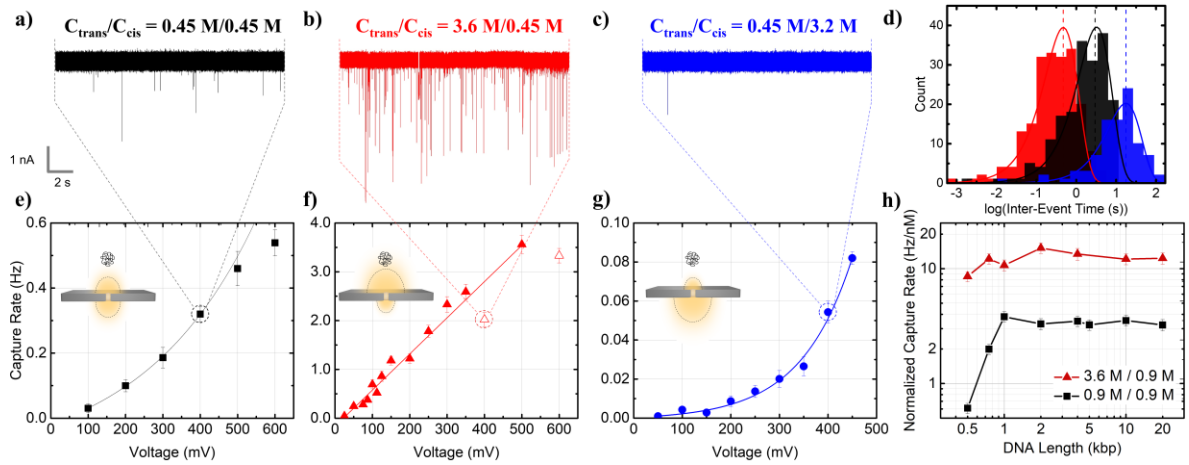

Figure 2. Comparison of capture kinetics in symmetric and asymmetric salt concentration conditions.

Representative ionic current traces for 0.25 nM of 10 kbp dsDNA under 400 mV in a 5.3 nm pore in a 10 nm thick SiN membrane under **(a)** symmetric salt conditions (0.45 M LiCl); **(b)** capture-promoting salt conditions (C_{trans}/C_{cis} > 1); **(c)** and capture-opposing salt conditions (C_{trans}/C_{cis} < 1). Data sampled at 4.17 MHz, analyzed, and displayed at 300 kHz with a low-pass Bessel filter. **(d)** Inter-event time distribution fitting for the data at 400 mV shown in a), b)

and c) with corresponding colors, where capture rate is extracted by fitting the log-transform of a Poisson distribution. **(e)** Voltage dependence of capture rate in SSC conditions (0.45 M LiCl, black squares); **(f)** capture-promoting ASC conditions ($C_{trans}/C_{cis} > 1$, red triangles); **(g)** and capture-opposing ASC conditions ($C_{trans}/C_{cis} < 1$, blue circles). **(h)** Normalized capture rate versus DNA length in an 8.5 nm pore in symmetric 0.9 M LiCl salt conditions (black squares) and 4x capture-promoting ASC conditions (red triangles) under a 400 mV bias. Error bars result from assuming Poisson statistics for capture rate uncertainty and a conservative 10% DNA concentration uncertainty. Note that some intra-pore capture rate variations are present, which we attribute to uncontrolled variability sources [33]. Data deemed as outliers are displayed as hollow, as shown in f), and ignored during fitting.

As a control, Figure 2e shows the voltage dependence of the capture rate of 10 kbp dsDNA in symmetric 0.45 M LiCl conditions for this 5.3 nm nanopore. A subtle nonlinear trend can be observed for $\Delta V \leq 400$ mV, which fits well to an exponential function. For $\Delta V > 400$ mV, the data does not fit well to an exponential fit and is expected instead to be described by a linear voltage dependence, as supported and discussed in the following section. These trends are expected from Equation 1 in SSC conditions [32,33,37,53], with the change of capture regime from barrier-limited to diffusion-limited occurring around $\Delta V^* \approx 400$mV.

Figure 2f shows the voltage dependence of the capture rate in the C_{trans}/C_{cis} = 3.6 M/0.45 M > 1 ASC condition on the same pore. As expected, the measured capture rates are appreciably higher than in SSC conditions (e.g. 3.56 Hz vs. 0.46 Hz at 500 mV). The capture rate in this capture-promoting case clearly exhibits a linear voltage dependence for the entire voltage range, characteristic of the diffusion-limited regime, even at very low voltages ($\Delta V^* < 50$ mV). Conversely, Figure 2g shows that when the polymer is located on the high salt concentration side of a comparable salt gradient (C_{trans}/C_{cis} = 0.45 M/3.2 M < 1), the capture rate is drastically reduced

and a clear exponential voltage dependence is observed throughout the entire voltage range investigated, characteristic of the barrier-limited regime (ΔV^*> 500 mV).

Next, we explored the scaling of capture with polymer length, by measuring the capture rates of dsDNA ranging from 500 to 20,000 bp in an 8.5 nm pore under a fixed 400 mV bias in two different LiCl salt conditions. Figure 2h shows the normalized capture rate J as a function of polymer length N for SSC (C_{trans}/C_{cis} = 0.9 M/0.9 M = 1) and capture-promoting ASC (C_{trans}/C_{cis} = 3.6 M/0.9 M = 4) conditions. In the SSC condition, as previously observed [32,33,37], the capture rate initially sharply increases with DNA length before exhibiting a length-independent behavior. For the experimental conditions used here, the regime-transition polymer length between the barrier-limited and the diffusion-limited regimes is $N^* \approx$ 1 kbp. In contrast, the 4× ASC condition shows a higher normalized capture rate with no such clear dependence on polymer length for the range studied. Only the shortest length tested, at N = 500 bp, may indicate the onset of a smooth transition towards a length-dependent regime. Although hard to pinpoint, the capture regime transition appears to be shifted toward shorter polymers in capture-promoting ASC conditions as compared to the SSC conditions.

From the capture rate results presented in Figure 2, we conclude that the dynamics of capture in ASC conditions are described by the same physical phenomena as in symmetric case: The barrier-limited and diffusion-limited regimes provide adequate descriptions of the properties of capture under ASC conditions. Moreover, ASC conditions demonstrate modulation of the transition between capture regimes, with capture-opposing gradients ($C_{trans}/C_{cis} < 1$) extending the barrier-limited transition to larger polymers and higher voltages, and capture-promoting gradients ($C_{trans}/C_{cis} > 1$) reducing the transition to shorter polymers and smaller voltages.

Capture Rate Modulation

Characterizing the extent to which capture rate is modulated by ASC conditions is of practical value for precise molecular counting applications. The data in Figure 2 and ensuing interpretation that salt gradients alter the capture-regime transitions suggest that the observed capture enhancement between different ASC conditions should also be capture-regime dependent.

To investigate this, we used the 10 kbp dsDNA data from Figure 2e-f to calculate the capture rate enhancement R_{ASC}/R_{SSC} between the capture-promoting ASC (C_{trans}/C_{cis} = 3.6 M/0.45 M >1) and SSC (C_{trans}/C_{cis}= 0.45 M/0.45 M = 1) conditions. Figure 3a displays the voltage dependence of the capture rate enhancement. Under a 100 mV bias, the capture rate enhancement is measured to be ~20-fold. Capture enhancement decreases with increasing voltages until ≈ 400 mV where it becomes approximately constant. For ≥ 400 mV, the value of the capture enhancement is approximately equivalent to the salt concentration or conductivity ratios of the *trans* and *cis* sides. This enhancement value was observed in previous work and is expected for the diffusion-limited regime [37,39]. This was attributed to the fact that the electric field far from the pore in ASC conditions is approximately enhanced by a factor of $\sigma_{trans}/\sigma_{cis} \approx C_{trans}/C_{cis}$, when compared to the SSC conditions. Interestingly, the voltage at which R_{ASC}/R_{SSC} plateaus to C_{trans}/C_{cis} coincides well with ΔV^*, the voltage at which capture appears to transition from barrier- to diffusion-limited under the SSC condition (Figure 2e). Note that in high salt concentration, electrical conductivity is not strictly linearly related to salt concentration [65]. Conductivity measurements across the various LiCl concentrations used here however show that $\sigma_{trans}/\sigma_{cis} \approx C_{trans}/C_{cis}$ is a reasonable approximation (see Section S1 of the Electronic Supplementary Material, ESM).

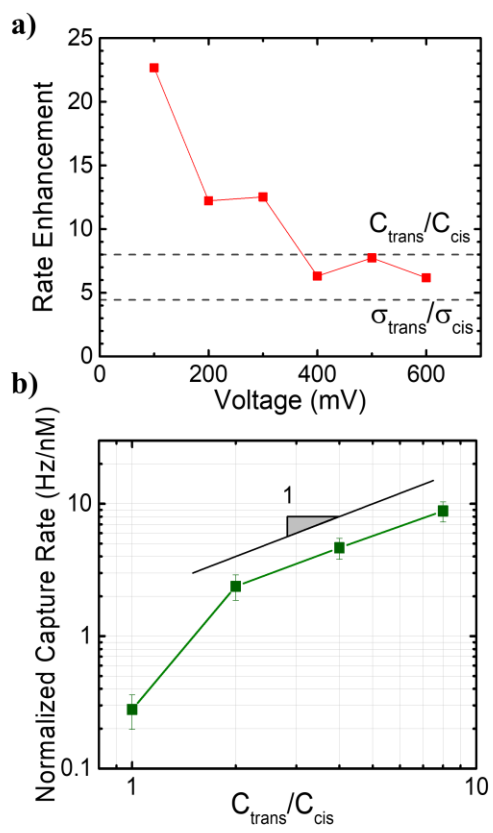

Figure 3. Regime-dependent capture enhancement. (a) Capture rate enhancement (R_{asc}/R_{ssc}) versus voltage using 10 kbp capture data in a 5.3 nm pore from Figure 2. **(b)** Capture rate versus C_{trans}/C_{cis} on a log-log scale, to better show the linear scaling for higher salt concentration ratios. Measurements done in a 5.1 nm pore, under a 200 mV bias, using 5 kbp dsDNA with C_{cis} fixed at 0.45 M LiCl.

We next measured the capture rate of 5 kbp dsDNA in a 5.1 nm pore, under a 200 mV bias, with C_{cis} fixed at 0.45 M LiCl and C_{trans} ranging from 0.45 M to 3.6 M LiCl. Figure 3b shows the normalized capture rate measured for different values of C_{trans}/C_{cis}. As expected from previous publications [37,39], capture rate grows monotonically with increasing salt-concentration ratios. Interestingly, a linear dependence of capture rate on C_{trans}/C_{cis} is observed for $C_{trans}/C_{cis} \geq 2$, whereas a super-linear trend is observed for smaller salt concentration gradients. As shown in

section S2 of the ESM, the transition from super-linear to linear dependence on C_{trans}/C_{cis} was observed under multiple experimental conditions [39].

Since increasing the applied voltage or the salt-concentration ratio increases the forces on the *cis*-side, both Figures 3a and 3b demonstrate that stronger cis-side forces promote diffusion-limited capture and result in a capture enhancement approximately equal in magnitude to C_{trans}/C_{cis}, whereas weaker forces promote barrier-limited capture and result in enhancements significantly higher than the salt concentration ratio C_{trans}/C_{cis}. We therefore infer that, for the data in Figure 3b and section S2 of the ESM, polymers in salt gradients ≥ 2 are in the diffusion-limited capture regime, whereas for smaller salt gradients polymers are in the barrier-limited capture regime.

Interestingly, the concept of regime-dependent capture enhancement appears to be a general feature of transport through nanopores as it also applies to non-linear polymers, such as DNA nanostructures [66]. In section S3 of the Electronic Supplementary Material (ESM), we show that the scaling of capture rate with C_{trans}/C_{cis} is different for two similar DNA nanostructures with different intrinsic rigidities. Because the nanostructures must deform and bend to pass through the pore, different rigidities result in different free-energy barriers. The more flexible structure, which experiences a lower free-energy barrier, is seen to scale almost linearly with C_{trans}/C_{cis}, indicating diffusion-limited capture. The more rigid structure, which experiences a higher free-energy barrier, scales super-linearly with the salt concentration ratio, indicating barrier-limited capture.

Translocation Time Scaling

In the second part of this work, in order to gain more insights into the physics of translocation, we investigate the scaling of translocation time τ with applied voltage and polymer

length in both ASC and SSC conditions. Translocation dynamics are commonly characterized through the scaling coefficients α and β of translocation time with polymer length and applied voltage, respectively [29]:

$$\tau \sim N^{\alpha} \Delta V^{\beta} \quad (2)$$

Tension propagation (TP) models dictate that the length-scaling coefficient α should be bounded by 1 and 1+ν, where ν = 0.588 is the Flory exponent for free-draining polymers, and the voltage-scaling coefficient β should be equal to -1 for free-draining polymers (equivalently, the mean translocation velocity, ν, should be linearly dependent on the applied voltage) [25,26,61].

We first investigated the scaling of translocation time with applied voltage $\tau \sim \Delta V^{\beta}$ by using the same data as that of Figure 2e-g, for 10 kbp dsDNA translocating through a 5.3 nm pore under applied voltages ranging from 50 mV to 600 mV in SSC (C_{trans}/C_{cis} = 0.45 M/0.45 M = 1), capture-promoting ASC (C_{trans}/C_{cis} = 3.6 M/0.45 M > 1), and capture-opposing ASC (C_{trans}/C_{cis} = 0.45 M/3.2 M < 1) conditions. Figure 4a shows the translocation times measured at various voltages for these three conditions. Interestingly, translocation times measured in both capture-promoting and capture-opposing ASC conditions are longer than in SSC conditions for all applied voltages. As expected from IFTP theory [25,27–29], translocation times in SSC conditions exhibit an inversely proportional voltage-scaling, as identified by the slope of $\beta = -1.04 \pm 0.08$ measured on the log-log plot of Figure 4a. Translocation times from both ASC conditions appear to display a scaling coefficients of -1 at high voltages (here for $\Delta V >$ ~200 mV), but for lower voltages, the coefficients deviate as seen by the non-constant slopes in the log-log plot ($\beta < -1$ for capture-opposing, and $\beta > -1$ for capture-promoting ASC conditions). To explain this behavior, we plotted the translocation velocity ($\nu = 0.34\, nm \times N/\tau$) as a function of voltage for both ASC

conditions (Figure 4b). Just like SSC conditions, translocation velocity exhibits a linear dependence on voltage, with linear fits of the form $v = a\Delta V + v_0$. An equivalent linear fit for the translocation time versus voltage, $\tau = 0.34 \times N/(a\Delta V + v_0)$, is included in the log-log plot of Figure 4a and fits remarkably well the data over the entire voltage range. Unlike SSC conditions, translocation velocities in ASC conditions have nonzero intercepts v_0, i.e. nonzero translocation velocities with no voltage applied: Capture-promoting conditions results in an intercept of $v_0 = +1.4 \pm 0.2\ nm/\mu s$, whereas capture-opposing conditions in $v_0 = -1.3 \pm 0.2\ nm/\mu s$.

Note that with no applied voltage, the only forces acting on dsDNA should be solely of diffusioosmotic and diffusiophoretic origin, as discussed above (Figure 1). The intercepts obtained from the linear fits should therefore correspond to the velocity induced by these forces. Interestingly, the fact that both values are comparable in magnitude but opposite in sign indicates that the salt gradient across the nanopore alone induces a force on DNA pointing from the low-salt-concentration side to the high-salt-concentration side, resulting in a translocation velocity of $v < 2\frac{nm}{\mu s}$. The direction of the force therefore suggests that diffusiophoresis is more important than diffusioosmosis in our experimental configuration (see Figure 1b). Furthermore, this zero-voltage velocity is in good agreement with the diffusiophoretic translocation velocity values obtained by McMullen *et al*. [56] under similar experimental conditions. Figures 4a-b and the corresponding linear fits therefore show that the $\tau \sim \Delta V^{-1}$ scaling is maintained under ASC conditions, albeit with an extra diffusiophoretic force which causes a non-zero translocation velocity under no applied voltage and is responsible for the non-constant slopes observed in log-log plot of Figure 4a.

Next, to experimentally verify the scaling of translocation time with polymer length $\tau \sim N^{\alpha}$ under ASC condition (C_{trans}/C_{cis} = 3.6 M/0.9 M = 4), we used dsDNA of lengths ranging from 500 bp to 48 kbp translocating through three 8.5 nm ± 1 nm diameter pores under a 400 mV bias and compared it to a SSC (C_{trans}/C_{cis} = 0.9 M/0.9 M = 1) control experiment. The measured translocation times are plotted in Figure 4c, which shows slower translocations in capture-promoting ASC conditions than in SSC conditions, consistent with Figure 4a. Fitting the data to power-scaling law functions of the form of Equation 2 yielded scaling coefficients of α_{SSC} = 1.22 ± 0.02 for SSC and α_{ASC} = 1.10 ± 0.07 for ASC condition (fits shown in section S4 of the ESM). While the extracted α_{SSC} coefficient is in very good agreement with a handful of values reported in previous experimental studies [34,67,68], the scaling coefficient in ASC conditions, α_{ASC}, is significantly smaller than α_{SSC} (P = 0.06, obtained using a Welch t-test). To our knowledge, such a scaling reduction, albeit more drastic, has been only reported when comparing translocation times of DNA entering and exiting a glass nanopipette [69].

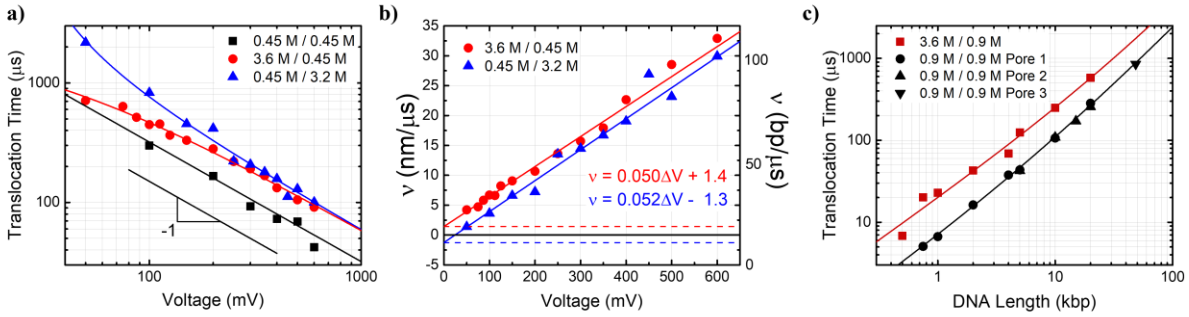

Figure 4. Translocation kinetics in ASC and SSC conditions. **(a)** Log-log plot of translocation time versus voltage in SSC (black squares), capture-promoting (red circles), and capture-opposing (blue triangles) ASC conditions. All data is from 10 kbp dsDNA in the same 5.3 nm pore. Solid lines show the optimal fits to functions of the form $\tau = (a\Delta V + b)^{-1}$. **(b)** ASC condition data from (a) replotted to show translocation velocity versus voltage. Solid lines are the same linear fits showed in (a). **(c)** Log-log plot of translocation time versus polymer length for symmetric (red squares, C_{trans}/C_{cis} = 0.9 M/0.9 M) and 4x capture-promoting ASC (black circles, triangles C_{trans}/C_{cis}

= 3.6 M/0.9 M) conditions, under 400 mV in 8.5 ± 1 nm pores. Red square and black circle data were acquired from the same nanopore. Continuous curves are fits to Equation 4 (for fits to Equation 2 see Figure S4 in the ESM). **(b)** *i)* Translocation time versus voltage in SSC, *ii*) capture-promoting ($C_{trans}/C_{cis} > 1$) and *iii*) capture-opposing ($C_{trans}/C_{cis} < 1$) ASC conditions.

Theoretical studies and simulations of tension propagation have shown that a simple power-law expression in the form of Equation 2 is insufficient to capture the length-dependence of translocation times [27,28,60,61,70]. To incorporate finite polymer-length effects and pore friction, models such as the Iso-Flux Tension Propagation (IFTP) [28] propose a length-dependence correction of the form

$$\tau = AN^{1+\nu} + BN \tag{3}$$

where A and B are simple coefficients whose values depend on pore geometry, solution viscosity, and pulling force inside the pore. The first term results from the drag of monomers on the *cis*-side and is expected to dominate for long polymers. The second term results from the polymer-pore interactions and is expected to dominate for short polymers. Note that this two-term scaling is equivalent to having a length-dependent scaling coefficient $\alpha(N)$ in Equation 2, where translocations dominated by pore friction ($A \ll B$) result in $\alpha \approx 1$, and translocations dominated by *cis*-side monomer drag ($A \gg B$) result in $\alpha \approx 1.588$. To experimentally verify the validity of Equation 3, the translocation times of Figure 4c were fitted using the equivalent but more insightful form

$$\tau = \frac{t_c}{2}\left[\left(\frac{N}{N_c}\right)^{\kappa} + \frac{N}{N_c}\right] \tag{4}$$

with t_c, N_c and κ as free parameters, allowing the extraction of κ, the scaling coefficient of *cis*-side monomers, and N_c the crossover length at which both the *cis*-monomer friction term and pore-friction term contribute equally to a translocation time of t_c. Note that κ is left as a free parameter in order to verify the IFTP prediction of κ = 1.588 [28]. From the optimal fits shown in Figure 4c, we extracted scaling coefficients of $\kappa_{ssc} = 1.53 \pm 0.10$ and $\kappa_{asc} = 1.61 \pm 1.49$, and crossover lengths of $N_C^{ssc} = 10 \pm 6$ kbp and $N_C^{asc} = 52 \pm 89$ kbp in SSC and ASC conditions, respectively. Both κ values correspond within error to the expected theoretical value of $\kappa = 1+\nu = 1.588$, although with significantly higher uncertainty for κ_{asc}. Moreover, the higher value and higher uncertainty of N_C^{asc} indicate that the fitting of ASC data is insensitive to the first term of Equation 4, *i.e.* the *cis*-monomer drag term. A broader range of polymer lengths covering both sides of the transition point would be necessary to reduce the uncertainty on this parameter.

Interestingly, a higher N_c value implies that the kinetics of translocation are more dominated by polymer-pore interactions in ASC conditions than in SSC conditions [27,28,60]. This conclusion is consistent with the reduction of the scaling parameter α observed for the simple power-law fits of Equation 2. Figure 4c and its corresponding fits therefore show that polymer translocations in ASC and SSC conditions are well described by IFTP, albeit with different relative contributions from *cis*-side and pore-polymer drag forces.

Modulation of Translocation Time Statistics

We now attempt to gain insights into how ASC conditions alter polymer conformations during steps *ii* and *iii* of capture in Figure 1b, the steps prior to translocation during which polymers are elongated and compressed by the forces outside the pore, respectively. Since a polymer's conformation directly impacts its translocation time [71], this section is devoted to studying the

effects of ASC conditions on the distribution of translocation times, i.e. the higher-order statistics of translocation times. To achieve this, we measured the passage times of 10 kbp dsDNA in a 6.0 nm pore, under a 300 mV bias, with C_{cis} fixed at 1.8 M LiCl and C_{trans} ranging from 0.9 M to 3.6 M LiCl.

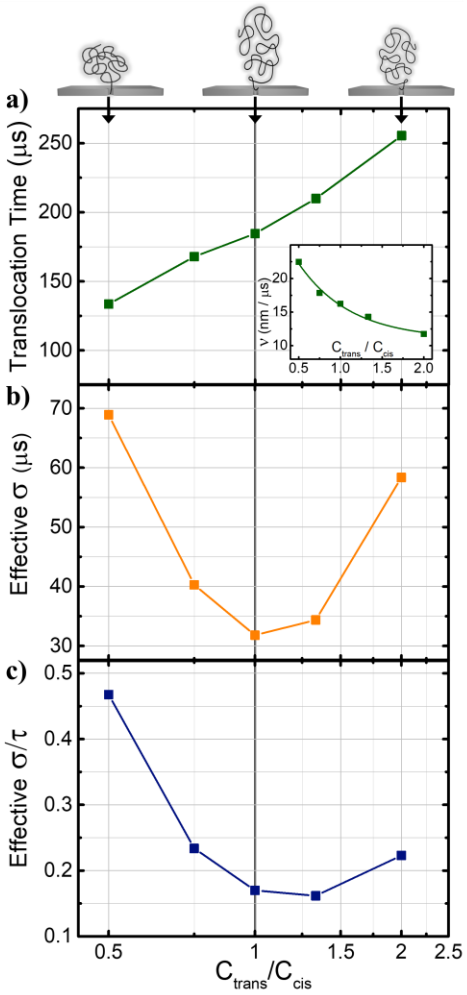

Figure 5. Dependence of 10 kbp translocation time statistics on salt concentration ratios for fixed C_{cis} =1.8M LiCl and varying C_{trans} under 300 mV in a 6.0 nm pore. **(a)** Mean Translocation time, **(b)** Translocation time standard deviation, and **(c)** Translocation time coefficient of variation versus C_{trans}/C_{cis} on semi-log *x*-scale. The inset of (a) shows the corresponding translocation velocity versus C_{trans}/C_{cis}. Schematics of the deduced polymer elongations in different ASC conditions are shown above (a).

Figure 5a and its inset plot the dependence of the mean translocation time τ and velocity $\mathcal{v}$ on the salt concentration ratio C_{trans}/C_{cis}, respectively. For the entire range tested, τ monotonically increases (i.e. $\mathcal{v}$ decreases) with C_{trans}/C_{cis} for both capture-promoting ($C_{trans}/C_{cis} > 1$) and capture-opposing ($C_{trans}/C_{cis} < 1$) ASC conditions, with τ seeing a twofold increase in going from C_{trans}/C_{cis} = 0.5 to 2. Velocity and force being proportional, it can be concluded that the pulling force inside the pore, responsible for driving the translocation process, reduces with C_{trans}/C_{cis}.

As discussed earlier (see Figure 1), the reduction of the pulling force inside the pore with C_{trans}/C_{cis} should be a direct result of diffusiophoretic and electrophoretic force modulations under different salt concentration gradients. Note that translocation velocities reduce by >10 nm/μs in going from C_{trans}/C_{cis} = 0.5 to 2 (23 nm/μs vs 12 nm/μs, respectively), as shown in the inset of Figure 5a. This velocity change is significantly higher than the <2 nm/μs diffusiophoretic contribution estimated in Figure 4b, but also in the opposite direction: Diffusiophoresis induces DNA motion from the lower to the higher salt concentration reservoir, with higher gradients resulting in higher velocities. Electrophoresis is therefore more likely responsible for slower translocations, and can be altered in two ways by salt gradients: The non-uniform conductivity can modulate the electric field (Figure 1c), and the local salt concentration inside the pore can alter DNA's mobility during translocation. Due to symmetry, the voltage drop across the pore for a C_{trans}/C_{cis} = 0.5 salt gradient should be the same as for a C_{trans}/C_{cis} = 2 gradient, and be maximal for C_{trans}/C_{cis} = 1. The salt-gradient-induced field modulation should therefore contribute non-monotonically to the translocation times, which is inconsistent with observations from Figure 5a. The most likely primary source of translocation time modulation is therefore the local concentration inside the pore modulating the electrophoretic mobility of dsDNA, for which slower translocations are expected in higher salt concentrations [46,47]. This is further supported by the

dependence of translocation time velocity $\mathcal{v}$ on salt gradient C_{trans}/C_{cis} being well described by a decaying exponential (fit shown in Figure 5a inset), a dependence previously reported by Rivas *et al* [47].

Since the spread of translocation times is a measure of the conformational entropy of polymers at the onset of translocation [67,71], we next investigated its dependence on C_{trans}/C_{cis}. To achieve this, we extracted the effective standard deviation σ from the 10 kbp dsDNA translocation time distributions and calculated the effective coefficient of variation σ/τ in different ASC conditions, as shown in Figures 5b and 5c. Unlike translocation times, σ exhibits a convex non-monotonic dependence on C_{trans}/C_{cis}, with a minimum located near $C_{trans}/C_{cis} = 1$. As a result, the σ/τ values are asymmetric around $C_{trans}/C_{cis} = 1$ with the capture-promoting ASC conditions resulting in significantly smaller σ/τ values than their inverse capture-opposing conditions. Note that since ASC conditions increase the fraction of folded translocations (analysis shown in section S5 of Electronic Supplementary Material), the effective spread of translocation times were instead extracted from the population of folded translocations (see Methods and section S6 of ESM for description and validation of this method).

Previous studies have shown that polymers stretched prior to translocation display reduced conformational entropy (and σ/τ values) due to their more elongated conformations [67,72,73]. Interpreting σ/τ values as being inversely correlated with the average conformation elongation, Figure 5c could therefore show a non-monotonic relationship between elongation and salt concentration ratio C_{trans}/C_{cis}: For a fixed C_{cis} and varying C_{trans}, capture-opposing ASC conditions ($C_{trans}/C_{cis} < 1$) result in less elongated polymer conformations than SSC conditions ($C_{trans}/C_{cis} = 1$), which in turn result in more elongated conformations than capture-promoting ASC conditions ($C_{trans}/C_{cis} > 1$), with the maximal elongation occurring near $C_{trans}/C_{cis} = 1$ (see Figure 5d). To

further validate the increase of σ/τ in capture-promoting ASC conditions and support the proposed elongation interpretation, the dependence of σ and σ/τ on polymer length is shown and analyzed in section S7 of the Electronic Supplementary Material, in which a similar σ/τ increase is observed.

Insights from Observations

Multiple observations and claims regarding nanopore capture and translocation dynamics in ASC and SSC conditions were brought forward in the four previous sections, including that capture-promoting ASC conditions promote diffusion-limited capture, whereas capture-opposing ASC conditions promote barrier-limited capture, and that polymers translocating under capture-promoting ASC conditions are slower than in SSC conditions, more dominated by pore friction and are more elongated than under SSC conditions. We now discuss how these observations converge to paint a complete picture of the nanopore transport process, consistent with what was described in Figure 1.

First, to better assess the change in dynamics when going from SSC to ASC conditions, we address the most plausible mechanisms by which electrophoretically-driven capture and translocation are altered in the presence of salt gradients. Figures 4 and 5a showed that salt-gradient-mediated electrophoretic mobility modulation is the main contribution to translocation time variations in ASC conditions. This explains why translocations occurring from the low salt side C_{low} or high salt side C_{high} of a given salt gradient are of similar durations and are both slower than translocations in SSC conditions (Figure 4), and why translocation time increases monotonically with C_{trans}/C_{cis} when C_{cis} is kept fixed, i.e. as the average salt concentration inside the pore increases (Figure 5a). We caution that while this is true of our experimental conditions,

for which diffusiophoretic forces are less important than electrophoretic ones (Figure 4b), this might not be the case for experiments using lower voltages (<100 mV), lower aspect ratio pores (d/L<1), or even in lower salt concentrations (<0.1 M) in which overlapping Debye layers introduce more complex behavior [45].

Interestingly, the reduction of the pulling force inside the pore in capture-promoting ASC conditions ($C_{trans}/C_{cis} > 1$ Figure 4 and 5a) makes it harder for polymers to successfully cross the entropic-based free-energy barrier, and fully translocate the nanopore. Although this appears to be at odds with the observation that ASC conditions promote diffusion-limited capture, a capture regime independent of the energy barrier (Figure 2), we believe it instead highlights the role that forces outside the pore play on the capture process: Strong attractive forces on the *cis*-side access region make it hard for DNA molecules to diffuse away from the pore and therefore promote successful translocations by virtue of increased time spent near the pore. Since capture-promoting ASC conditions are expected to increase the *cis*-side forces mainly due to increased electrophoretic pull (Figure 1c), we therefore suggest that salt-gradient-modulated electric fields outside the pore are directly responsible for ASC conditions promoting diffusion-limited ($C_{trans}/C_{cis} > 1$) or barrier-limited ($C_{trans}/C_{cis} < 1$) capture regimes.

In order to better understand the non-monotonic trend of translocation time spread vs C_{trans}/C_{cis} (Figure 5c), and to support the interpretation that polymer conformations in ASC conditions are less elongated than in SSC conditions, we next discuss how the force modulations in ASC conditions are expected to impact the polymer conformations prior to successfully entering and threading through the pore, i.e. during steps *ii* and *iii* of Figure 1d. As per the above discussion, the monotonic increase of capture rate with salt gradient (Figure 3b) shows that forces outside the pore increase monotonically with C_{trans}/C_{cis}. Due to the forces being non-uniform and strongest

near the pore, polymers are radially elongated as they approach the pore, i.e. during step *ii* of Figure 1d. Since stronger forces can result in stronger stretching, we expect the elongation of polymers throughout step *ii* to increase monotonically with C_{trans}/C_{cis}. Subsequently, once the polymer reaches the pore mouth and attempts to initiate translocation by surmounting the free-energy barrier, i.e. during step *iii* of Figure 1d, it is actively being compressed against the membrane by the forces outside the pore. The duration of step *iii*, and therefore the amount of time during which a polymer is compressed, is closely related to the magnitude of the pulling force inside the pore. A strong pulling force, for example, should facilitate crossing the free-energy barrier and therefore reduce the time required for a polymer to initiate translocation. As a result, a weaker force should promote polymer compression, as it provides more time for forces outside the pore to compress the polymer, whereas the opposite is true for strong pulling forces. Since Figure 5a showed that the pulling force inside the pore reduces monotonically with C_{trans}/C_{cis} for fixed C_{cis}, we conclude that increasing C_{trans}/C_{cis} has two confounding effects on polymer conformations: it promotes elongation during step *ii*, and promotes compression during step *iii*.

We believe that these elongation and compression phenomena explain the non-monotonic translocation time σ/τ values shown in Figures 5b,c: For $C_{trans}/C_{cis} \gg 1$, although polymers arrive at the pore with highly elongated conformations due to strong forces outside the pore, they have time to be significantly compressed prior to threading due to the same strong outside forces and the weak forces inside the pore. For $C_{trans}/C_{cis} < 1$, polymers are not significantly elongated when arriving at the pore, nor are they significantly compressed due to the weaker *cis*-side forces and stronger forces inside the pore. Note that there exists a value of C_{trans}/C_{cis} that naturally results in maximal elongation during translocation, by optimally balancing pre-stretching and compression. For the current experimental conditions, this value empirically occurs at a salt ratio slightly higher

than 1, as demonstrated by the minimal σ/τ value of Figure 5c. This minimum in translocation time spread, surprisingly close to C_{trans}/C_{cis} = 1, corresponds to the optimized experimental condition under which molecules can be characterized and separated.

Finally, the concept of ASC conditions inducing less-elongated conformations is consistent with the observations from Figure 4a, where in fitting translocation times to Equations 2 and 4, we concluded that translocations in ASC conditions (C_{trans}/C_{cis} = 3.6 M / 0.9 M) were more pore-friction dominated than in SSC conditions (C_{trans}/C_{cis} = 0.9 M / 0.9 M), or equivalently that *cis*-side monomer friction was less dominant than in SSC. More elongated conformations are indeed expected to result in more significant *cis*-side monomer friction throughout the translocation steps *iv* and *v* [28,71]. This is simply due to more elongated conformations having more monomers under tension and in motion soon after translocation begins, with the limiting case being a completely stretched-out polymer with end monomers moving almost instantly as translocation begins. We therefore believe that the scaling coefficient reduction observed in ASC conditions is a direct consequence of polymers being less elongated prior to translocation.

3. Conclusion

We presented an extensive description of DNA capture and translocation dynamics through characterization of the dependence of capture rate, translocation time statistics, and folding kinetics (shown in section S5 of the ESM), on voltage, polymer length, and salt concentration gradient.

We showed that the underlying physics describing the transport process in asymmetric salt concentration (ASC) conditions is the same as in symmetric salt concentrations (SSC). The barrier-

and diffusion-limited capture regimes combined with tension propagation principles fully describe the capture and translocation process. The promotions of diffusion- or barrier-limited regimes in capture-promoting or –opposing ASC conditions respectively demonstrated that the *cis*-side electric field plays a crucial role in determining capture kinetics. The higher order statistics of translocation time distributions further confirmed experimentally that non uniform forces outside the pore are responsible for elongating and compressing polymers before and after reaching the pore mouth, respectively.

This work confirmed the previously published conclusions[37,39–45] that detecting molecules from the low salt-concentration side of a salt gradient increases capture rate, slows down translocation, and increases the signal-to-noise ratio through deeper blockage depths (latter not shown). Although these are ideal features for nanopore sensing, we also observed an increase in the spread of the translocation times (Figure 5a), an increase in the percentage of folded translocations (Figure S5 of the ESM), and significantly more frequent pore clogs when working in capture-promoting ASC conditions. The increased folding and translocation time spread can be undesirable for applications requiring single-file passage, such as DNA-carrier-based bioassays and data storage applications which require mapping with the highest precision objects bound to linear polymers. The biggest drawback however to ASC conditions may probably be the likelihood of permanent pore clogs, occurring more frequently than in symmetric conditions, and therefore significantly reducing the lifespan and usability of nanopores. For asymmetric salt concentration conditions to be of practical use in different applications, this issue should be addressed, possibly by employing different coating strategies and types of surface chemistries [74,75] to control polymer-pore interactions.

Finally, we hope that our results will provide motivation for further theoretical work on the capture and translocation processes. We believe that consideration of the electric field outside the pore and its role in elongating and compressing polymers should help bridge theoretical and experimental efforts. Namely, elucidating the impact of field-induced polymer conformations on the translocation time scaling with polymer length will help develop a thorough understanding of the nanopore transport process, which will be essential in guiding development of nanopore-based applications in numerous critical fields.

4. Experimental Methods

Nanopore Fabrication. Nanopores were fabricated in 10 nm thick SiN membranes purchased from Norcada Inc. (NBPX5004Z-60O-Hi RES) using controlled breakdown, following the protocols and procedures outlined in detail in Waugh *et al* [76]. Concisely, pores were fabricated in 1 M KCl pH 8 using a linear voltage ramp, followed by conditioning to enlarge using 3 second 3 V pulses in 3.6 M LiCl pH 8, until the desired pore size was reached [77].

DNA Translocation Experiments. Ionic current traces were sampled using a Chimera VC100 at 4.167 MHz. After establishing a difference in salt concentration across the nanopore, a minimum of 30 minutes was allowed to elapse before applying a voltage and recording translocation events, to ensure a time-independent I-V curve (see Section S9 of the ESM), which we attribute to the ζ-potential of the pore walls and the ion distribution inside the pore reaching a steady state [78,79]. For all measurements, the voltage was adjusted in order to zero the current, therein nulling the effects of Nernst potentials, and of diffusio-osmosis [56] induced by a salinity gradient. The current signal is recorded for 10-15 minutes depending on the observed capture rate with the aim

of collecting at least 300 events. During the experiment, a zapping function was enabled which inverted the bias polarity for 3 seconds if the open pore conductance decreased by > 5% its original value indicating undesired clogging of the pore. Data acquired during zapping was ignored for analysis. DNA concentrations were ascertained using a spectrophotometer (Biotek Epoch 2). For experiments on a single pore, for which multiple voltages or DNA lengths were sampled, the experiment order was randomized as to not have time-dependent pore characteristics (e.g. growth) be responsible for changes in capture and translocation kinetics, instead of the varying voltage or DNA length. It should also be noted that only pores with stable conductance baselines (±5% change within experiments) were used.

Data Analysis. Current trace data is analyzed using a custom implementation of the CUSUM+ and adept2state algorithms (see https://github.com/shadowk29/CUSUM) [80]. Since capture inherently obeys Poisson process statistics, capture rates are extracted by fitting the histogram of the logarithm of inter-event times to the log-transform of the Poisson distribution function. A detailed description of the accuracy of this capture rate fitting method and other similar methods in different experimental conditions is provided in our previous work [33]. The mean translocation time of unfolded DNA and its standard deviation are extracted from experimental data in one of two ways: 1) Since unfolded translocation times are sufficiently well described by a log-normal distribution, a Gaussian fit is applied to the histogram of the logarithm of the translocation times, provided enough unfolded translocations are observed. The mean and standard deviation of translocation times are then calculated using well-known lognormal properties; 2) Since asymmetric salts significantly promotes folded translocations (see Figure S5 in the ESM), large sample sizes of unfolded events can be difficult to obtain. In such cases, we define the effective translocation time τ_{eff} to be the ratio of the equivalent charge deficit (ECD) and the single dsDNA

blockage level. Here, ECD denotes the integral of the ionic blockage with respect to the open-pore baseline. This approach mathematically unravels the blockage trace and can be used to faithfully increase the sample size of the mean unfolded translocation time. Section S6 of the ESM validates this second method by demonstrating that both methods quantitatively agree on the standard deviation of the translocation time distribution of a highly populated data set.

Electronic Supplementary Material

Supplementary material (Additional information regarding the non-linearity of salt-concentration and conductivity, the regime-dependent capture enhancement of linear DNA and DNA nanostructures, the different fits of translocation time and DNA length scaling, the folding statistics, the method for extracting higher-order translocation time statistics from folded translocations, the DNA-length dependence of higher order translocation time statistics, and the IV stabilization when going from SSC to ASC conditions.) is available in the online version of this article at http://dx.doi.org/10.1007/s12274-***-****-*

ACKNOWLEDGMENTS

The authors would like to acknowledge the support of the Natural Sciences and Engineering Research Council of Canada (NSERC), through funding from grant #CRDPJ 530554-18. The authors would also like to thank Kyle Briggs and Gary Slater for fruitful discussions.

REFERENCES

[1] Deamer, D., Akeson, M. & Branton, D. Three decades of nanopore sequencing. *Nat. Biotechnol.* 2016, **34**, 518–524.

[2] Logsdon, G. A., Vollger, M. R. & Eichler, E. E. Long-read human genome sequencing and

its applications. *Nat. Rev. Genet.* 2020, **21**, 597–614.

[3] Garalde, D. R. *et al.* Highly parallel direct RNA sequencing on an array of nanopores. *Nat. Methods* 2018, **15**, 201–206.

[4] Branton, D. *et al.* The potential and challenges of nanopore sequencing. *Nat. Biotechnol.* 2008, **26**, 1146–1153.

[5] Lindsay, S. The promises and challenges of solid-state sequencing. *Nat. Nanotechnol.* 2016, **11**, 109–111.

[6] Xue, L. *et al.* Solid-state nanopore sensors. *Nat. Rev. Mater.* 2020, **5**, 931–951.

[7] Bell, N. A. W. & Keyser, U. F. Digitally encoded DNA nanostructures for multiplexed, single-molecule protein sensing with nanopores. *Nat. Nanotechnol.* 2016, **11**, 645–651.

[8] Chuah, K. *et al.* Nanopore blockade sensors for ultrasensitive detection of proteins in complex biological samples. *Nat. Commun.* 2019, **10**,.

[9] Sze, J. Y. Y., Ivanov, A. P., Cass, A. E. G. & Edel, J. B. Single molecule multiplexed nanopore protein screening in human serum using aptamer modified DNA carriers. *Nat. Commun.* 2017, **8**, 1–10.

[10] Raveendran, M., Lee, A. J., Sharma, R., Wälti, C. & Actis, P. Rational design of DNA nanostructures for single molecule biosensing. *Nat. Commun.* 2020, **11**, 1–9.

[11] Morin, T. J. *et al.* A handheld platform for target protein detection and quantification using disposable nanopore strips. *Sci. Rep.* 2018, **8**, 14834.

[12] Varongchayakul, N., Song, J., Meller, A. & Grinstaff, M. W. Single-molecule protein sensing in a nanopore: a tutorial. *Chem. Soc. Rev.* 2018, **47**, 8512–8524.

[13] Yusko, E. C. *et al.* Real-time shape approximation and fingerprinting of single proteins using a nanopore. *Nat. Nanotechnol.* 2016, **12**, 360–367.

[14] Ouldali, H. *et al.* Electrical recognition of the twenty proteinogenic amino acids using an aerolysin nanopore. *Nat. Biotechnol.* 2020, **38**, 176–181.

[15] Nivala, J., Marks, D. B. & Akeson, M. Unfoldase-mediated protein translocation through an α-hemolysin nanopore. *Nat. Biotechnol.* 2013, **31**, 247–250.

[16] Alfaro, J. A. *et al.* The emerging landscape of single-molecule protein sequencing technologies. *Nat. Methods* 2021, **18**, 604–617.

[17] Brinkerhoff, H., Kang, A. S. W., Liu, J., Aksimentiev, A. & Dekker, C. Multiple rereads of single proteins at single-amino acid resolution using nanopores. *Science* 2021, **374**, 1509–1513.

[18] Schmid, S., Stömmer, P., Dietz, H. & Dekker, C. Nanopore electro-osmotic trap for the label-free study of single proteins and their conformations. *Nat. Nanotechnol.* 2021, **16**, 1244–1250.

[19] Lucas, F. L. R., Versloot, R. C. A., Yakovlieva, L., Walvoort, M. T. C. & Maglia, G. Protein identification by nanopore peptide profiling. *Nat. Commun.* 2021, **12**, 1–9.

[20] Chen, K. *et al.* Digital Data Storage Using DNA Nanostructures and Solid-State Nanopores. *Nano Lett.* 2019, **19**, 1210–1215.

[21] Cao, C. *et al.* Aerolysin nanopores decode digital information stored in tailored macromolecular analytes. *Sci. Adv.* 2020, **6**, 2–10.

[22] Boukhet, M. *et al.* Translocation of Precision Polymers through Biological Nanopores. *Macromol. Rapid Commun.* 2017, **38**, 1–6.

[23] Muthukumar, M. Theory of capture rate in polymer translocation. *J. Chem. Phys.* 2010, **132**,.

[24] Rowghanian, P. & Grosberg, A. Y. Electrophoretic capture of a DNA chain into a nanopore. *Phys. Rev. E - Stat. Nonlinear, Soft Matter Phys.* 2013, **87**, 1–8.

[25] Rowghanian, P. & Grosberg, A. Y. Force-Driven Polymer Translocation through a Nanopore: An Old Problem Revisited. *J. Phys. Chem. B* 2011, **115**, 14127–14135.

[26] Saito, T. & Sakaue, T. Dynamical diagram and scaling in polymer driven translocation. *Eur. Phys. J. E* 2011, **34**, 135.

[27] Ikonen, T., Bhattacharya, A., Ala-Nissila, T. & Sung, W. Influence of non-universal effects on dynamical scaling in driven polymer translocation. *J. Chem. Phys* 2012, **137**, 85101.

[28] Sarabadani, J., Ikonen, T. & Ala-Nissila, T. Iso-flux tension propagation theory of driven polymer translocation: The role of initial configurations. *J. Chem. Phys.* 2014, **141**, 214907.

[29] Palyulin, V. V., Ala-Nissila, T. & Metzler, R. Polymer translocation: The first two decades and the recent diversification. *Soft Matter* 2014, **10**, 9016–9037.

[30] Dubbeldam, J. L. A., Rostiashvili, V. G., Milchev, A. & Vilgis, T. A. Forced translocation of a polymer: Dynamical scaling versus molecular dynamics simulation. *Phys. Rev. E* 2012, **85**, 41801.

[31] Davenport, M. *et al.* The role of pore geometry in single nanoparticle detection. *ACS Nano* 2012, **6**, 8366–8380.

[32] Bell, N. A. W. W., Muthukumar, M. & Keyser, U. F. Translocation frequency of double-stranded DNA through a solid-state nanopore. *Phys. Rev. E - Stat. Nonlinear, Soft Matter Phys.* 2016, **93**, 1–10.

[33] Charron, M., Briggs, K., King, S., Waugh, M. & Tabard-Cossa, V. Precise DNA Concentration Measurements with Nanopores by Controlled Counting. *Anal. Chem.* 2019, **91**, 12228–12237.

[34] Storm, A. J. *et al.* Fast DNA translocation through a solid-state nanopore. *Nano Lett.* 2005, **5**, 1193–1197.

[35] van Dorp, S., Keyser, U. F., Dekker, N. H., Dekker, C. & Lemay, S. G. Origin of the electrophoretic force on DNA in solid-state nanopores. *Nat. Phys.* 2009, **5**, 347–351.

[36] Carson, S., Wilson, J., Aksimentiev, A. & Wanunu, M. Smooth DNA Transport through a Narrowed Pore Geometry. *Biophys. J.* 2014, **107**, 2381–2393.

[37] Wanunu, M., Morrison, W., Rabin, Y., Grosberg, A. Y. & Meller, A. Electrostatic focusing of unlabelled DNA into nanoscale pores using a salt gradient. *Nat. Nanotechnol.* 2010, **5**, 160–165.

[38] Chen, K. *et al.* Dynamics of driven polymer transport through a nanopore. *Nat. Phys.* 2021, **17**, 1043–1049.

[39] Jeon, B. J. & Muthukumar, M. Polymer capture by α-hemolysin pore upon salt concentration gradient. *J. Chem. Phys.* 2014, **140**,.

[40] Ivica, J., Williamson, P. T. F. & de Planque, M. R. R. Salt Gradient Modulation of MicroRNA Translocation through a Biological Nanopore. *Anal. Chem.* 2017, **89**, 8822–8829.

[41] Nova, I. C. *et al.* Investigating asymmetric salt profiles for nanopore DNA sequencing with biological porin MspA. *PLoS One* 2017, **12**, 1–14.

[42] Bello, J. *et al.* Increased dwell time and occurrence of dsDNA translocation events through solid state nanopores by LiCl concentration. *Electrophoresis* 2019, **40**, 1082–1090.

[43] He, Y. *et al.* Mechanism of how salt-gradient-induced charges affect the translocation of DNA molecules through a nanopore. *Biophys. J.* 2013, **105**, 776–782.

[44] Chou, T. Enhancement of charged macromolecule capture by nanopores in a salt gradient. *J. Chem. Phys.* 2009, **131**,.

[45] He, Y., Tsutsui, M., Scheicher, R. H., Miao, X. S. & Taniguchi, M. Salt-Gradient Approach for Regulating Capture-to-Translocation Dynamics of DNA with Nanochannel Sensors. *ACS Sensors* 2016, **1**, 807–816.

[46] Kowalczyk, S. W., Wells, D. B., Aksimentiev, A. & Dekker, C. Slowing down DNA translocation through a nanopore in lithium chloride. *Nano Lett.* 2012, **12**, 1038–1044.

[47] Rivas, F., DeAngelis, P. L., Rahbar, E. & Hall, A. R. Optimizing the sensitivity and resolution of hyaluronan analysis with solid-state nanopores. *Sci. Rep.* 2022, **12**, 1–10.

[48] Verschueren, D. V., Jonsson, M. P. & Dekker, C. Temperature dependence of DNA translocations through solid-state nanopores. *Nanotechnology* 2015, **26**, 234004.

[49] Farahpour, F., Maleknejad, A., Varnik, F. & Ejtehadi, M. R. Chain deformation in translocation phenomena. *Soft Matter* 2013, **9**, 2750–2759.

[50] Vollmer, S. C. & De Haan, H. W. Translocation is a nonequilibrium process at all stages: Simulating the capture and translocation of a polymer by a nanopore. *J. Chem. Phys.* 2016, **145**,.

[51] Qiao, L. & Slater, G. W. Ratcheting charged polymers through symmetric nanopores using pulsed fields: Designing a low pass filter for concentrating DNA. *arXiv preprint* 2021, arXiv.2101.12712.

[52] Seth, S. & Bhattacharya, A. How capture affects polymer translocation in a solitary nanopore. *J. Chem. Phys.* 2022, **156**, 244902.

[53] Nakane, J., Akeson, M. & Marziali, A. Evaluation of nanopores as candidates for electronic analyte detection. *Electrophoresis* 2002, **23**, 2592–2601.

[54] Gershow, M. & Golovchenko, J. A. Recapturing and trapping single molecules with a solid-state nanopore. *Nat. Nanotechnol.* 2007, **2**, 775–779.

[55] Wong, C. T. A. A. & Muthukumar, M. Polymer capture by electro-osmotic flow of oppositely charged nanopores. *J. Chem. Phys.* 2007, **126**,.

[56] McMullen, A., Araujo, G., Winter, M. & Stein, D. Osmotically Driven and Detected DNA Translocations. *Sci. Rep.* 2019, **9**, 1–10.

[57] Rankin, D. J., Bocquet, L. & Huang, D. M. Entrance effects in concentration-gradient-driven flow through an ultrathin porous membrane. *J. Chem. Phys.* 2019, **151**,.

[58] Lee, C. *et al.* Osmotic flow through fully permeable nanochannels. *Phys. Rev. Lett.* 2014, **112**, 1–5.

[59] Anderson, J. Colloid Transport By Interfacial Forces. *Annu. Rev. Fluid Mech.* 1989, **21**, 61–99.

[60] Ikonen, T., Bhattacharya, A., Ala-Nissila, T. & Sung, W. Influence of pore friction on the universal aspects of driven polymer translocation. *Europhysics Lett.* 2013, **103**, 38001.

[61] Ikonen, T., Bhattacharya, A., Ala-Nissila, T. & Sung, W. Unifying model of driven polymer translocation. *Phys. Rev. E - Stat. Nonlinear, Soft Matter Phys.* 2012, **85**, 1–7.

[62] Sakaue, T. Dynamics of polymer translocation: A short review with an introduction of weakly-driven regime. *Polymers (Basel).* 2016, **8**, 1–12.

[63] Meller, A., Nivon, L. & Branton, D. Voltage-driven DNA translocations through a nanopore. *Phys. Rev. Lett.* 2001, **86**, 3435–3438.

[64] Stellwagen, N. C., Gelfi, C. & Righetti, P. G. The free solution mobility of DNA. *Biopolymers* 1997, **42**, 687–703.

[65] Tanaka, K. & Reita Tamamushi. A Physico-chemical Study of Concentrated Aqueous Solutions of Lithium Chloride. *Zeitschrift für Naturforsch. A* 1991, **8**, 55.

[66] He, L., Karau, P. & Tabard-Cossa, V. Fast capture and multiplexed detection of short multi-arm DNA stars in solid-state nanopores. *Nanoscale* 2019, **11**, 16342–16350.

[67] Briggs, K. *et al.* DNA Translocations through Nanopores under Nanoscale Preconfinement. *Nano Lett.* 2018, **18**, 660–668.

[68] Mihovilovic, M., Hagerty, N. & Stein, D. Statistics of DNA capture by a solid-state nanopore. *Phys. Rev. Lett.* 2013, **110**, 1–5.

[69] Bell, N. A. W., Chen, K., Ghosal, S., Ricci, M. & Keyser, U. F. Asymmetric dynamics of DNA entering and exiting a strongly confining nanopore. *Nat. Commun.* 2017, **8**, 380.

[70] Sarabadani, J. *et al.* Driven translocation of a semi-flexible polymer through a nanopore. *Sci. Rep.* 2017, **7**, 1–8.

[71] Lu, B., Albertorio, F., Hoogerheide, D. P. & Golovchenko, J. A. Origins and consequences of velocity fluctuations during DNA passage through a nanopore. *Biophys. J.* 2011, **101**, 70–79.

[72] de Haan, H. W., Sean, D. & Slater, G. W. Reducing the variance in the translocation times by prestretching the polymer. *Phys. Rev. E* 2018, **98**, 22501.

[73] Sean, D., de Haan, H. W. & Slater, G. W. Translocation of a polymer through a nanopore starting from a confining nanotube. *Electrophoresis* 2015, **36**, 682–691.

[74] Bandara, Y. M. N. D. Y., Karawdeniya, B. I., Hagan, J. T., Chevalier, R. B. & Dwyer, J. R. Chemically Functionalizing Controlled Dielectric Breakdown Silicon Nitride Nanopores by Direct Photohydrosilylation. *ACS Appl. Mater. Interfaces* 2019, **11**, 30411–30420.

[75] Eggenberger, O. M., Ying, C. & Mayer, M. Surface coatings for solid-state nanopores. *Nanoscale* 2019, **11**, 19636–19657.

[76] Waugh, M. *et al.* Solid-state nanopore fabrication by automated controlled breakdown. *Nat. Protoc.* 2020, **15**, 122–143.

[77] Beamish, E., Kwok, H., Tabard-Cossa, V. & Godin, M. Precise control of the size and noise of solid-state nanopores using high electric fields. *Nanotechnology* 2012, **23**, 405301.

[78] Lin, C.-Y. *et al.* Modulation of Charge Density and Charge Polarity of Nanopore Wall by Salt Gradient and Voltage. *ACS Nano* 2019, **13**, 9868–9879.

[79] Firnkes, M. *et al.* Electrically facilitated translocations of proteins through silicon nitride nanopores: conjoint and competitive action of diffusion, electrophoresis, and electroosmosis. *Nano Lett.* 2010, **10**, 2162–2167.

[80] Forstater, J. H. J. H. *et al.* MOSAIC: A modular single-molecule analysis interface for decoding multistate nanopore data. *Anal. Chem.* 2016, **88**, 11900–11907.